PCCP

ARTICLE TYPE

Cite this: 10.1039/D3CP02571C

New Prebiotic Molecules in the Interstellar Medium from the Reaction Between Vinyl Alcohol and CN Radical†: Unsupervised Reaction Mechanism Discovery, Accurate Electronic Structure Calculations and Kinetic Simulations

Bernardo Ballotta,*[a] Emilio Martínez-Núñez,[b] Sergio Rampino,[c] and Vincenzo Barone*[a]

Vinyl alcohol (VyA) and cyanide radical (CN) are relatively abundant in the interstellar medium (ISM). VyA is the enolic tautomer of acetaldehyde and has two low-lying conformers, characterized by the *syn* or *anti* placement of the hydroxyl hydrogen with respect to the double bond. In this paper, we present a gas-phase model of the barrierless reactions of both VyA's conformers with CN employing accurate quantum chemical computations in the framework of a master equation approach based on the transition state theory.Our results indicate that both VyA's conformers feature a similar reactivity with CN, starting with a barrierless addition to the double bond and followed by different isomerization, dissociation, and/or hydrogen elimination steps. The rate constants computed for temperatures up to 600 K show that several reaction channels are open even in the harsh conditions of the ISM, with the favoured one providing the first feasible formation route of a prebiotic molecule not yet detected in the ISM, namely cyanoacetaldehyde. This finding suggests to look for cyanoacetaldehyde in regions where both VyA and CN have been already detected, like, e.g., Sagittarius B2N or G+0.693-0.027.

1 Introduction

In the last decades, thanks to ever more precise detection systems, such as radio telescopes and satellites, more than 200 molecules have been detected in the interstellar medium (ISM)[1]. The census includes an increasing number of so-called interstellar complex organic molecules (iCOMs), i.e. molecules containing at least one carbon atom and not less than 6 atoms. Some of these species are supposed to be the chemical precursors of life bricks, like amino acids or nucleobases[2,3]. Given the low amount of dust present in the ISM (about 1%), gas-phase reactions may play a central role in the formation of iCOMs[4]. However, only reaction channels involving submerged transition states (TSs) are open in the ISM due to its very low temperature and pressure. The unusual chemistry characterizing this environment is driven by the attack of highly reactive ionic and radical species to suitable targets, which leads to the formation of increasingly complex species[5]. However, despite the ever increasing efforts that have been made to understand how iCOMs can be produced in the ISM, only few formation routes have been unequivocally characterized till now. In this connection, simulations of reaction mechanisms and computational kinetics investigations are playing an increasing role thanks to the development of accurate quantum chemical (QC) and kinetic models[6]. From these analyses it is also possible to obtain theoretical parameters useful for the simulation of the evolution of astrophysical objects (e.g., the molecular clouds, which represent the initial stages of star formation processes), whose chemistry is still poorly known.

Based on these premises, we have performed a comprehensive computational study of the reaction between vinyl alcohol (VyA) and cyanide radical (CN), two species, which have been detected in several regions of the ISM. In particular, VyA's microwave transitions have been detected in emission toward the dense molecular cloud Sagittarius B2(N) (SgrB2N)[7]. VyA is the enolic form of acetaldehyde, and both tautomers belong to the family of C_2H_4O isomers together with oxirane (also identified in the ISM). VyA

[a] *Scuola Normale Superiore, Piazza dei Cavalieri 7, 56126 Pisa, Italy. E-mail: bernardo.ballotta@sns.it, vincenzo.barone@sns.it*

[b] *Departamento de Química Física, Facultade de Química, Campus Vida, Universidade de Santiago de Compostela, Avenida das Ciencias s/n, 15782, Santiago de Compostela, Spain.*

[c] *Università degli Studi di Padova, Dipartimento di Scienze Chimiche, Via Marzolo 1, 35131 Padova, Italy. Also at: Istituto Nazionale di Fisica Nucleare, Sezione di Pisa, Largo Bruno Pontecorvo 3, 56127 Pisa, Italy.*

† Electronic Supplementary Information (ESI) available:In the PDF file we have collected: Cartesian coordinates and relative energies of all critical points, plots of the barrierless reaction steps and MESS input files. See DOI: 10.1039/cXCP00000x/

can exist in two rotameric forms, corresponding to the *syn* or *anti* arrangement of the hydroxyl hydrogen with respect to the double bond[8]. Over the years much work has been devoted to the spectroscopic characterization of VyA and its presence in various astronomical objects has been researched[9,10]. Possible reaction mechanisms have also been hypothesized using experimental and computational approaches to account for the relative abundances of the *syn* and *anti* isomers[11–13]. Furthermore, enols and aldehydes are considered key tracers of a non-equilibrium chemistry driven by cosmic rays leading to complex organic molecules[14]. The CN radical has also been detected in SgrB2N and in other regions of the ISM[15] and it is possibly involved in several gas-phase reaction mechanisms for the formation of iCOMs (see, for instance, Refs.[16–19]).

We present here a comprehensive computational analysis for the gas-phase barrierless reactions of both VyA's conformers with CN, which, to the best of our knowledge, has been never investigated before. Based on previous experience, reaction mechanisms have been produced using automated research methods to have a more detailed exploration of the possible chemical reaction pathways[20]. Then, the thermochemistry and kinetics of the reactions have been characterized by a QC approach, which integrates double hybrid functionals and wave-function composite schemes[21,22]. Our results indicate that *anti* and *syn* conformers feature a similar, but not identical reactivity with CN. The reactions start with a barrierless addition to the VyA double bond, which leads to the formation of very stable reaction intermediates, lying well below the reactant asymptote. After that, for both isomers the reaction can evolve towards the formation of several products through isomerization and dissociation steps which lead to the formation of several molecular species with only some of them having been already detected in the ISM. Rate constants have been next computed in a range of temperatures typical of the ISM. According to the kinetic simulations, the most favoured products for both conformers are cyanoacetaldehyde (a prebiotic molecule not yet detected in the ISM, but for which several formation routes have been proposed[23,24]) and the dissociation product composed by vinylcyanide and hydroxyl radical, both of which have been already detected in the ISM.

The article is organized as follows. In Section 2, the computational methods are described. In Section 3, the computed reaction mechanisms are discussed with reference to the stationary points of the potential energy surface (PES). In Section 4, the kinetics of the reactions is addressed. Section 5 is devoted to conclusions.

2 Computational Details

2.1 Reaction mechanism discovery

All the reaction mechanisms discussed in the following have been automatically generated by means of the AutoMeKin[25–27] (AMK) program. Most programs for the automatic discovery of reaction mechanisms involve the initial optimization of energy minima and then the characterization of transition states (TSs). The methodology on which AMK is built is based instead on the initial optimization of the structures of TSs and the successive identification of the couple of energy minima connected by each TS by following the corresponding intrinsic reaction coordinate (IRC)[28]. The overall AMK workflow relies on the combination of molecular dynamics (MD) simulations, post-processing and selection of the TS molecular structures obtained with MD and the re-optimization of the molecular structures through DFT calculations. MD simulations have been performed using the semi-empirical PM7 method[29] implemented in the MOPAC software[30]. Geometry optimizations and zero-point corrected electronic energies of reactants, transition states, intermediates, and products along the reaction pathways have been obtained by the rev-DSD-PBEP86[31]-D3BJ[32] double-hybrid functional in conjunction with the jun-cc-pVTZ basis set[33] (here after this combination of functional and basis set will be referred to as rDSD). All the critical points belonging to the reaction pathways have been characterized as minima (reactants, intermediates and products) and saddle points (transition states) based on vibrational frequency calculations. The nature of saddle points has been further confirmed using intrinsic reaction coordinate (IRC)[28] scans at the same level of theory. The results of the simulations have been analyzed using amk_tools[34], a graphic visualizer, which allows the examination of the extremely complex reaction networks generated by AutoMeKin, the visualization of molecular structures with their vibrational normal modes and the check of the potential energy profiles for the investigated reaction mechanisms. A typical reaction network drawn by amk_tools is shown in Figure 1. Thanks to amk_tools, it has been possible to select all the structures of the critical points involved in the reaction pathways. For such structures, improved electronic energies have been obtained by exploiting the junChS-F12 composite scheme, which will be explained in more detail in the next subsection.

2.2 Electronic structure calculations

It is well known that for systems not showing strong multireference character the coupled-cluster (CC) model including single, double and (perturbatively) triple excitations (CCSD(T))[35] leads to an accurate estimation of electronic energies if complete basis set (CBS) extrapolation and core valence (CV) correlation are taken into proper account. The basic idea of the family of reduced-cost 'Cheap' composite schemes[21,36–38] is that single point CCSD(T) energy evaluations at rDSD geometries provide sufficiently accurate results employing a (partially augmented) triple-zeta basis set[33,39–41] and estimating CBS and CV contributions by means of second order Møller-Plesset theory (MP2). Average absolute errors of the order of 1 kJ mol^{-1} on reaction and activation energies have been reported for the most accurate jun-ChS-F12 variant (employed in the present paper) in which conventional methods are replaced by their explicitly correlated (F12) counterparts[42,43]. Anharmonic zero-point vibrational energy corrections have been computed in the framework of second-order vibrational perturbation theory[44] employing rDSD anharmonic force fields. All the rDSD calculations have been performed using the Gaussian package[45], while the junChS-F12 calculations have been performed using the MOLPRO program[46–48].

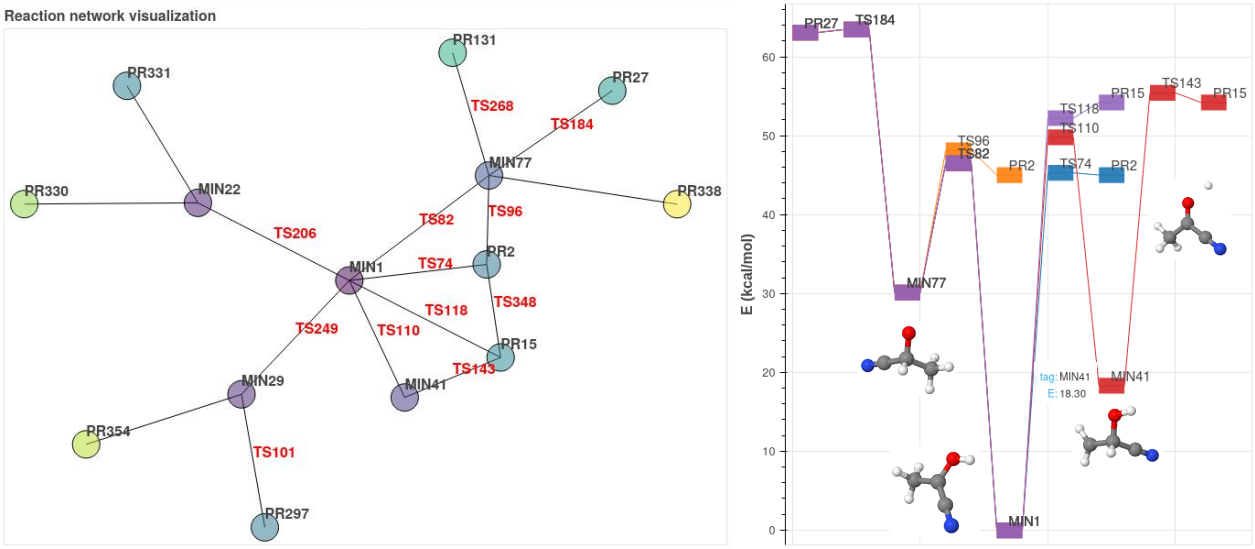

Fig. 1 An example of reaction network (left-side) and reaction profile (right-side) generated by amk_tools. The circles are the energy minima of the reaction network, while the connecting lines are the TSs.

2.3 Kinetics

Global and channel specific rate constants have been computed in the framework of the Ab Initio Transition State Theory based Master Equation (AITSTME) approach with the help of the MESS software[49]. In details, the multiwell one-dimensional master equation has been solved by the chemically significant eigenvalue (CSE) method with bimolecular products and reactants treated as sources and sinks. The phase space theory (PST)[50,51] has been employed to compute rate constants for barrierless steps in the approximation that the long-range interaction between the incoming reactants is described by an isotropic attractive potential $V(R) = -C_6/R^6$[52]. The C_6 parameters for both *anti* and *syn* conformers (63.49 and 64.09 $a_0^6 E_h$, respectively) have been obtained by a least-square fit of rDSD electronic energies computed at different values of the NC-CH_2CHOH distance. The rate coefficients of the elementary steps governed by distinct transition states have been computed by the conventional transition-state theory (TST). All the calculations have been carried out in the framework of the rigid-rotor harmonic-oscillator (RRHO) approximation and including tunneling as well as non-classical reflection effects using the Eckart model[53]. For all the transition states internal rotation (IR) modes have been identified by the use of redundant internal coordinates. For each IR, rotation potentials have been calculated by means of constrained scans. Depending on the nature and number of IR modes identified in the TSs, one-dimensional decoupled hindered rotor models or, in the case of internal rotations coupled with other rotation modes, multi-dimensional rotors have been employed. Kinetic simulations have been performed under the conditions typical of different regions of the ISM, namely a pressure of 10^{-8} bar and temperatures ranging between 10 and 600 K. The temperature dependence of the resulting rate constants has been fitted by a three-parameter modified Arrhenius equation, namely the Arrhenius–Kooij expression[54,55]:

$$k(T) = A(\frac{T}{300})^n e^{-\frac{E}{RT}}$$

where R is the universal gas constant, whereas A (pre-exponential factor), n, and E are the fitting parameters. The above equation is based on a linear variation of the activation energy (E_a) with the temperature, ($E_a/R = E + nT$), which, as we will see, is not a good approximation for some reaction channels.

3 Results

We start the presentation of the results by illustrating the reaction mechanism for the abstraction and addition reactions. Next, overall and channel-specific rate constants will be discussed. Since, all reactions start with a barrierless attack of CN to VyA, Figure 2 shows the results of the scan performed for this step. Other possible reaction channels (e.g., approach by the N (instead of C) end of CN, or different substitutions) have been identified in the initial search, but they have been discarded since preliminary computations revealed high energy barriers for at least one of the involved elementary steps.

3.1 Mechanism of abstraction reactions

Hydrogen abstraction from *syn*-VyA can lead to the formation of hydrogen cyanide together with four different radical species, **s-P1A**, **s-P2A**, **s-P3A**, and **s-P4A**.

Inspection of the reaction profile sketched in Figure 3 shows that the initial step is the formation of the intermediate **s-Int1A** lying 225.9 kJ mol^{-1} below the reactants. Starting from this intermediate the reaction can further proceed through 4 different transition states, **s-TS1A**, **s-TS2A**, **s-TS3A** and **s-TS4A**, corresponding to the attack of the **CN** radical to the four non-equivalent hydrogen atoms of *syn*-VyA. The lowest energy barrier (**s-TS1A**) lies 181.7 kJ mol^{-1} above **s-Int1A** (44.2 kJ mol^{-1} below the reactants) and governs the abstraction of the hydroxyl hydrogen. The transition states ruling the other hydrogen abstractions are **s-TS2A**, **s-TS3A**, and **s-TS4A**, which lie 247.0, 234.4, and 222.7 kJ mol^{-1} above the intermediate **s-Int1A**. The high energy barriers governing these three processes indicate that formation of **s-P1A**

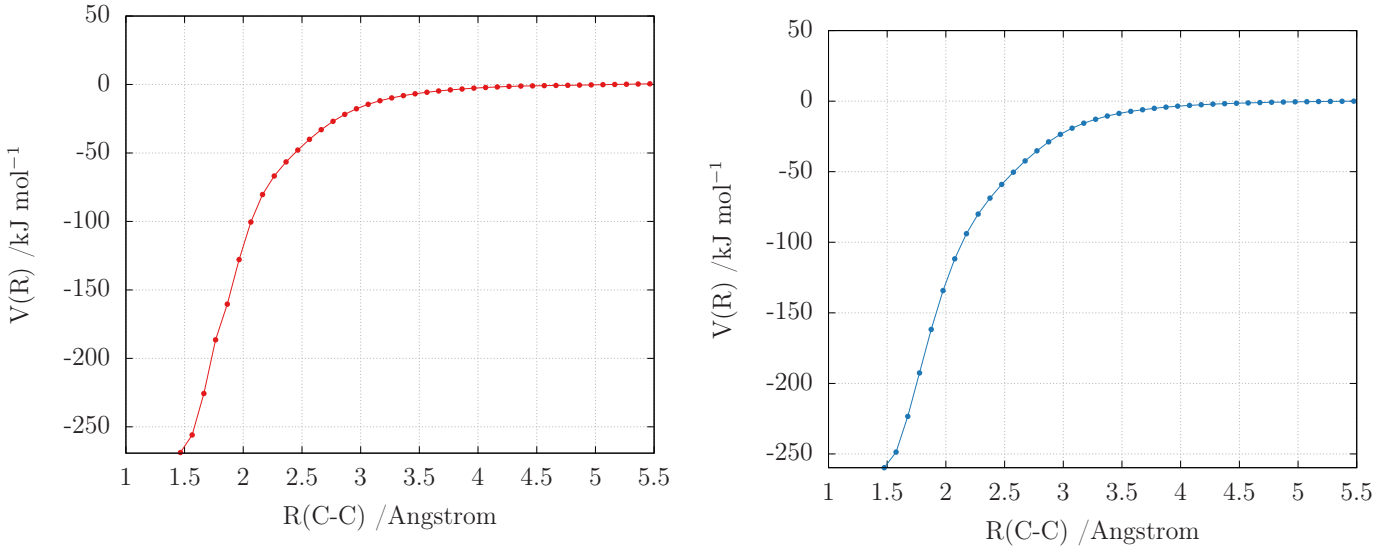

Fig. 2 One-dimensional potential energy "curves" as a function of C−C bond formation (Å) for the reactions *anti*-VyA + CN ⟶ a-Int1 in red and *syn*-VyA + CN ⟶ s-Int1 in blue computed at the rev-DSDPBEP86-GD3(BJ)/jun-cc-pVTZ level

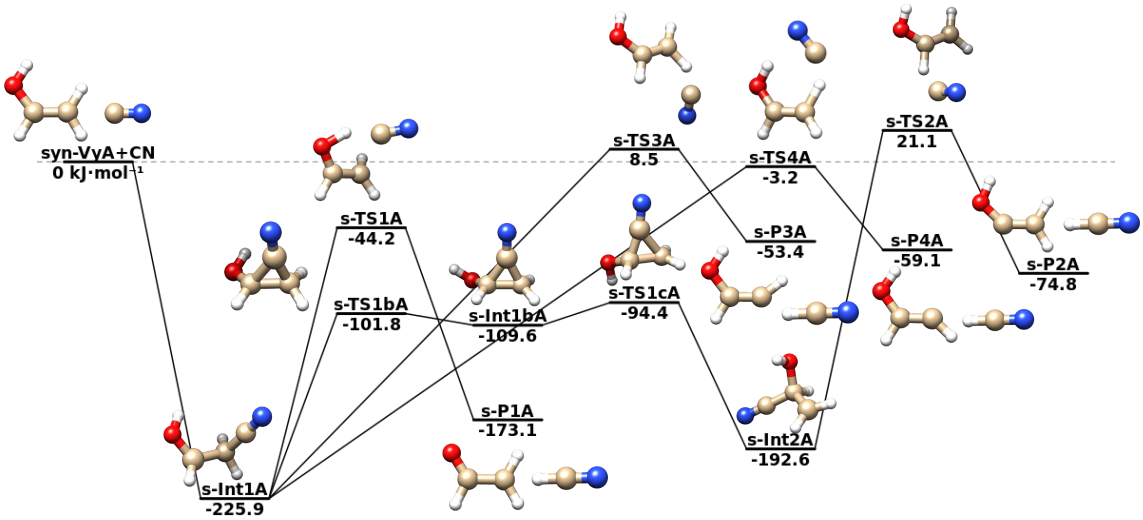

Fig. 3 Energetics of the abstraction reactions between *syn*-VyA and CN: junChS-F12 energies augmented by anharmonic rDSD ZPE corrections.

is kinetically favoured. Noted is that the same trend would be obtained in terms of thermodynamic control since **s-P1A** lies -173.1 kJ mol^{-1} below the reactants, whereas the exothermicity of the reactions leading to **s-P2A**, **s-P3A** and **s-P4A** are 74.8, 53.4, and 59.1 kJ mol^{-1}, respectively. The preference for the route leading to **s-P1A** can be traced back to the lower strength of the OH bond with respect to its CH counterparts and to the stabilization of the vinoxy radical (CH_2CHO) by π-electron delocalization in the C-C-O moiety.

In analogy with the case of *syn*-VyA, also the abstraction reactions involving the *anti* conformer start with the formation of a reaction intermediate **a-Int1A** lying 230.3 kJ mol^{-1} below the initial reactants. The reaction then proceeds through the attack of CN to one of the hydrogen atoms of *anti*-VyA overcoming the corresponding transition state (**a-TS1A**, **a-TS2A**, **a-TS3A**, or **a-TS4A**).

Inspection of the energy barriers collected in Figure 4 shows that the favored abstraction process leads to the formation of **a-P1A** following the **a-Int1A** ⟶ (**a-TS1A**) ⟶ **a-P1A** path. In fact **a-TS1A** is found 49.1 kJ mol^{-1} below the reactants, whereas **a-TS2A**, **a-TS3A** and **a-TS4A** lie 10.6, 6.9, and 7.7 kJ mol^{-1}, respectively above the reactants. All the reactions are exothermic, but all the paths except that leading to **a-P1A** are governed by energy barriers higher than the reactant asymptotic limit. As a consequence, the reactants would have to acquire a significant energy from the surrounding environment, with this being a highly unlikely process under the harsh conditions of the ISM.

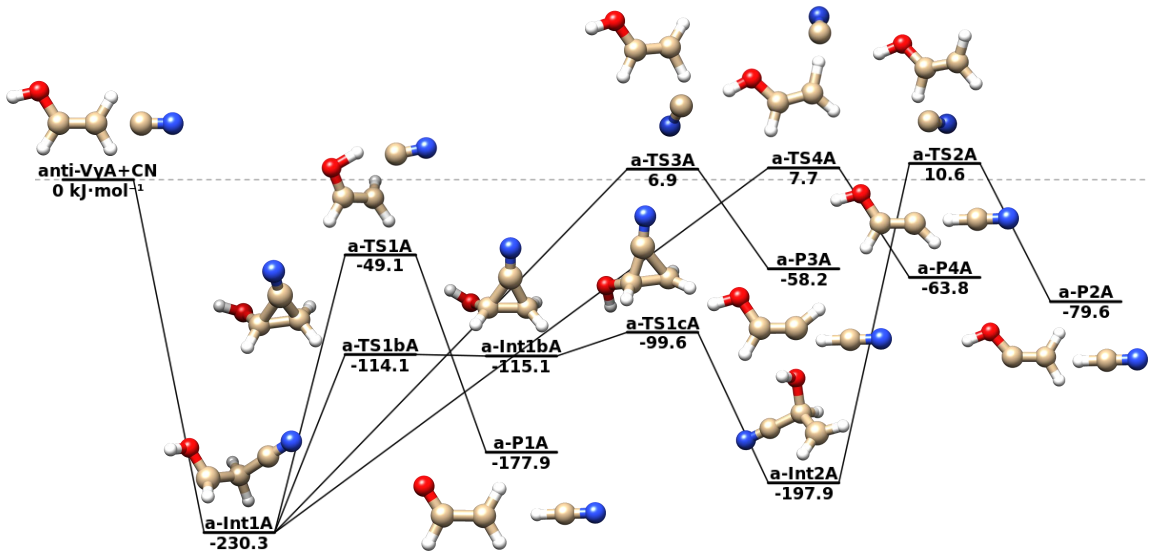

Fig. 4 Energetics of the abstraction reactions between the *anti*-VyA and CN: junChS-F12 energies augmented by anharmonic rDSD ZPE corrections.

3.2 Mechanism of addition reactions

The addition of CN to *syn*-VyA (see Figure 5) is characterized by an initial highly exothermic barrierless attack of CN to the double bond of *syn*-VyA which leads to the formation of the same intermediate **s-Int1** discussed above. The reaction can subsequently proceed with the elimination of atomic hydrogen through two different TSs, **s-TS4** at -73.1 kJ mol^{-1} and **s-TS8** at -68.1 kJ mol^{-1}, to form one of the isomers of cyanovinylalcohol (**s-P1**) at -94.3 kJ mol^{-1}, or cyanoacetaldehyde (**s-P3**) at -109.6 kJ mol^{-1}. Alternatively, the reaction can proceed with the transposition of hydrogen to form another more stable intermediate (**s-Int3**) at about -231.3 kJ mol^{-1} through **s-TS3** overcoming a barrier of 165.0 kJ mol^{-1}, or the transposition of the cyanide group via **s-Int1b** at -109.6 kJ mol^{-1} to arrive at the formation of **s-Int2** at about -192.6 kJ mol^{-1}.

After that, through several isomerization and dissociation paths, those three intermediates can lead to the formation of many other products, like two cyanovinylalcohol isomers (**s-P2** and **s-P7**) at -79.8 kJ mol^{-1} and -104.1 kJ mol^{-1}, respectively, vinylcyanide (**s-P6**) at -96.2 kJ mol^{-1}, formylcyanide (**s-P5**) at -110.7 kJ mol^{-1} and acetylcyanide (**s-P4**) at -114.2 kJ mol^{-1}. All those processes are strongly exothermic, a necessary condition for their feasibility in the ISM. It is also worth pointing out that only formylcyanide (**s-P5**)[56] and vinylcyanide (**s-P6**)[57] have been already detected in the ISM (in the SgrB2N region).

Also for *anti*-VyA the initial step corresponds to the barrierless attack of CN to the π system of VyA, leading to the formation of the reaction intermediate **a-Int1** at -230.3 kJ mol^{-1} (see Figure 6). From **a-Int1** the reaction can evolve through hydrogen elimination reactions to form **a-P1** at -98.6 kJ mol^{-1} and **a-P3** at -114.9 kJ mol^{-1}, passing through **a-TS4** and **a-TS8**, respectively. Otherwise **a-Int1** can evolve through isomerization steps which involve the transposition of the CN radical or the hydrogen atom through the **a-TS1** at -114.1 kJ mol^{-1} and **a-TS3** at -63.6 kJ mol^{-1} to form two others reaction intermediates, **a-Int2** at -197.9 kJ mol^{-1} and **a-Int3** at -234.7 kJ mol^{-1}. From **a-Int3**, another hydrogen elimination process can lead to the formation of **a-P7** through **a-TS5** with energy barrier of 157.8 kJ mol^{-1}.

From **a-Int2** a possible dissociation pathway can lead to the formation of **a-P6**, through **a-TS3b**. Also two isomerization steps can occur through hydrogen transposition mechanisms through **a-TS10** and **a-TS12**, which end with the formation of **a-Int4** at -273.2 kJ mol^{-1} and **a-Int5** at -175.1 kJ mol^{-1}. From **a-Int4** the hydrogen elimination can bring to the formation of **a-P4** through **a-TS13** with an energy barrier of 191.8 kJ mol^{-1}. From **a-Int5** two possible dissociation pathways can followed, which lead to the formation of **a-P4** and **a-P5** at -119.5 kJ mol^{-1} and -116.0 kJ mol^{-1} respectively.

Also in this case, although all the reaction channels are strongly exothermic, only some of the products have been already detected in the ISM, while many others (cyanoacetyladehyde (**a-P3**), isomers of cyanovinyl alcohol (**a-P1**, **a-P2**, **a-P7**) and acetylcyanide (**a-P4**)) have not yet been detected.

3.3 Rate constants

Before discussing in detail the different rate constants, let us recall that low-frequency torsional motions are present in most transition states and have been treated by different models depending on the value of the corresponding harmonic frequency and the extent of mode-mode coupling. Table 1 collects the specific models used for the different TSs.

As far as the tunnel effect is concerned, it can be hypothesized that it does not play an important role for the addition paths since all the TSs lie below the asymptotic limit of the reactants. The same comment can be made for the formation of the **P1A** and **P4A** products obtained from the *anti* and *syn* conformers of VyA, respectively. On the other hand, tunneling can affect the formation of **a-P2A**, **a-P3A** and **a-P4A** for the *anti* conformer and of **s-P2A** and **s-P3A** for the *syn* conformer. A general classification

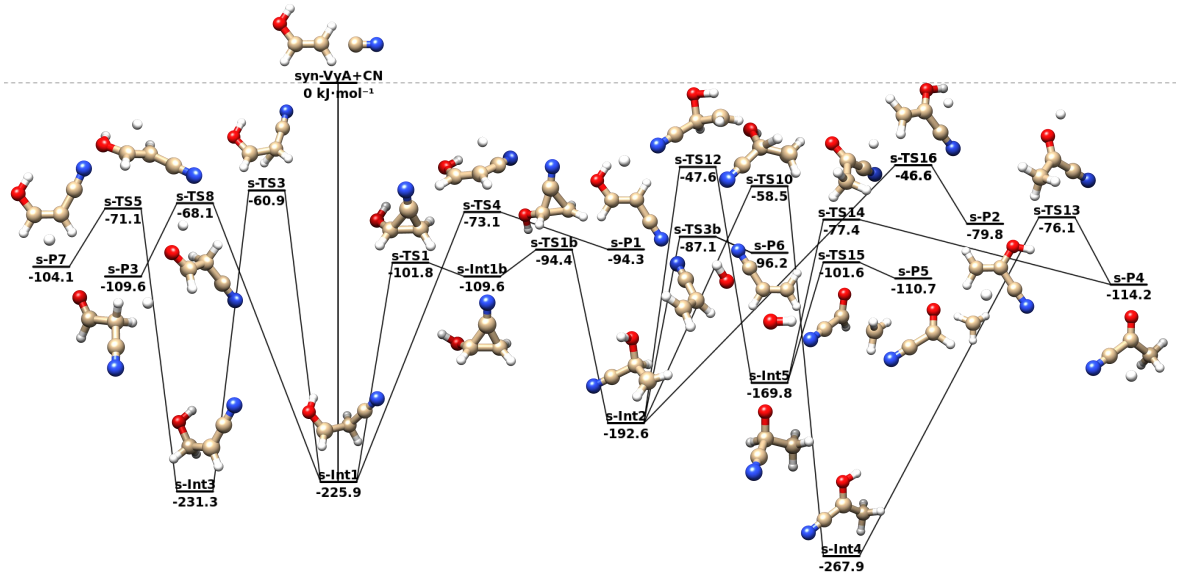

Fig. 5 Energetics of the addition reaction of CN to *syn*-VyA: junChS-F12 energies augmented by anharmonic rDSD ZPE corrections.

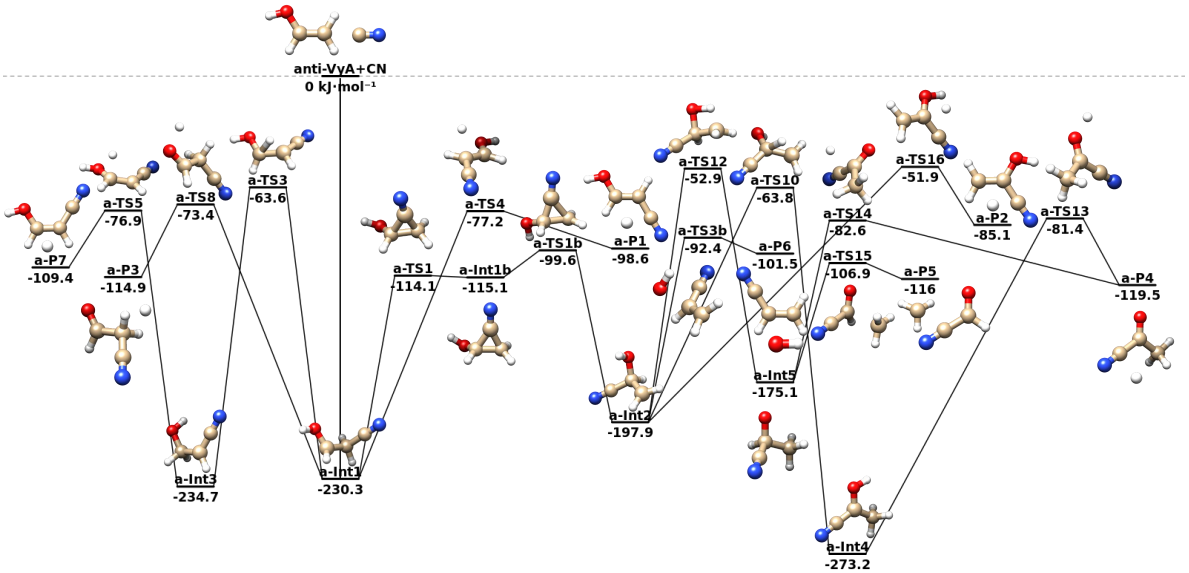

Fig. 6 Energetics of the addition reaction of CN to *anti*-VyA: junChS-F12 energies augmented by anharmonic rDSD ZPE corrections.

has been proposed for quantifying the role of tunneling in tuning rate constants[58]. For this purpose the "crossover temperatures", T_c have been calculated by using the following expression[59,60]

$$T_c = \frac{\hbar \nu^{\ddagger}}{R} \tag{1}$$

in which $\nu^{\ddagger}$ is the value of the imaginary frequency at the TS, R is the universal gas constant and $\hbar$ is the reduced Planck's constant. Depending on the value of T_c it is possible to define the tunneling regime of the various reactive paths in the investigated temperature range (T): classical, for $T > 4T_c$, negligible, for $4T_c > T > 2T_c$, moderate, for $2T_c > T > T_c$ and deep, for $T_c > T$.

In Table 2 are reported for both VyA's conformers the values of T_c for all the elementary steps governed by TSs lying above the reactants (i.e., those leading to the formation of **P2A**, **P3A** and **P4A**). The values show that for all the processes the tunneling regime ranges from deep to classical, except for the formation of **a-P2A** and **a-P4A** starting from *anti*-VyA, which ranges from moderate to classical. Although the presence of very stable reaction intermediates and of submerged TSs governing alternative channels suggest that tunneling should not alter decisively the overall reaction rates, this is not the case for channel-specific results and we will come back on this point after discussing the general trends of rate constants.

The Arrhenius plots for all the abstraction products **P1A**, **P2A**, **P3A**, **P4A** and the addition products **P1**, **P2**, **P3**, **P4**, **P5**, **P6**, **P7** for the reactions *syn*-VyA+CN and *anti*-VyA+CN, are shown in Figures 7, 8, 9 and 10. The parameters of the different fits are

anti-VyA + CN		*syn*-VyA + CN	
TS	**Model**	**TS**	**Model**
a-TS1	1D-HR	**s-TS1**	1D-HR
a-TS1b	1D-HR	**s-TS1b**	1D-HR
a-TS3	1D-HR	**s-TS3**	MD-HR
a-TS3b	MD-HR	**s-TS3b**	MD-HR
a-TS4	1D-HR	**s-TS4**	1D-HR
a-TS5	1D-HR	**s-TS5**	1D-HR
a-TS8	MD-HR	**s-TS8**	MD-HR
a-TS10	1D-HR	**s-TS10**	1D-HR
a-TS12	MD-HR	**s-TS12**	MD-HR
a-TS13	Free	**s-TS13**	Free
a-TS14	1D-HR	**s-TS14**	1D-HR
a-TS15	1D-HR	**s-TS15**	1D-HR
a-TS16	MD-HR	**s-TS16**	MD-HR
a-TS1A	Free	**s-TS1A**	Free
a-TS2A	Free	**s-TS2A**	Free
a-TS3A	Free	**s-TS3A**	Free
a-TS4A	Free	**s-TS4A**	Free

Table 1 List of the TSs involved in all the reaction mechanisms with the model used to treat the internal rotations, i.e., one-dimensional free rotor (Free), one-dimensional hindered rotor (1D-HR) and multi-dimensional coupled hindered rotors (MD-HR).

	T_c/K		T_c/K
s-P2A	16.6	**a-P2A**	17.9
s-P3A	34.7	**a-P3A**	36.2
s-P4A	39.5	**a-P4A**	26.1

Table 2 Crossover temperatures for the *syn*-VyA (left) and *anti*-VyA (right) abstraction processes.

given in Tables 7.7, 7.8, 7.9, 7.10 of the Supporting Information.

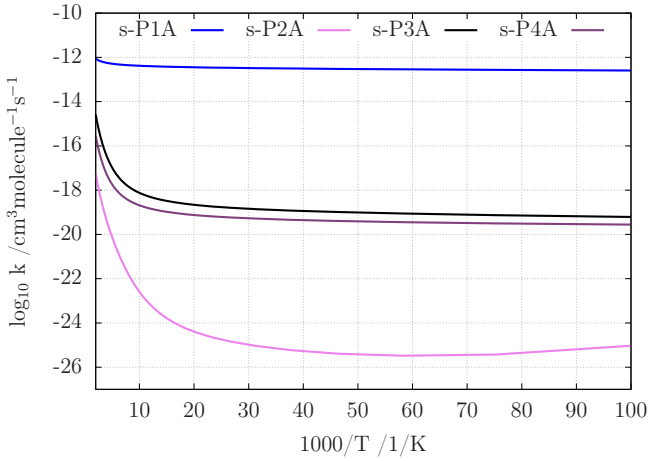

Fig. 7 Arrhenius plot of the formation rate constants of the products s-P1A, s-P2A, s-P3A, s-P4A of the *syn*-VyA + CN abstraction reactions.

Starting from abstraction reactions involving *syn*-VyA, inspection of the results reported in Figure 7 shows that the rate constant governing the formation of **s-P1A** (which ranges between 3.13×10^{-13} and 1.00×10^{-12} $cm^3molecule^{-1}s^{-1}$) is higher than the rate constants governing the formation of **s-P2A**, **s-P3A** and **s-P4A** in the whole interval of temperatures (10-600 K). The trend reflects the effect of the energy barriers and the nature of the reaction pathways leading to the various products. In fact, the formation pathways of **s-P1A** and **s-P4A** show submerged TSs lying 44.2 and 3.2 kJ mol^{-1} below the reactants, while **s-P2A** and **s-P3A** are reached through emerged TSs. Furthermore the formation of **s-P2A** involves three different intermediates and high energy barriers, which make it the most kinetically disfavoured process. The formation rate constant for the reaction channel leading to **s-P4A** ranges between 4.26×10^{-20} and 8.41×10^{-16} $cm^3molecule^{-1}s^{-1}$. For **s-P3A** it ranges between 1.11×10^{-19} and 8.05×10^{-15} $cm^3molecule^{-1}s^{-1}$. Finally, the rate constant governing the formation of **s-P2A** ranges between 1.62×10^{-32} and $5.36\times10^{-26}cm^3molecule^{-1}s^{-1}$.

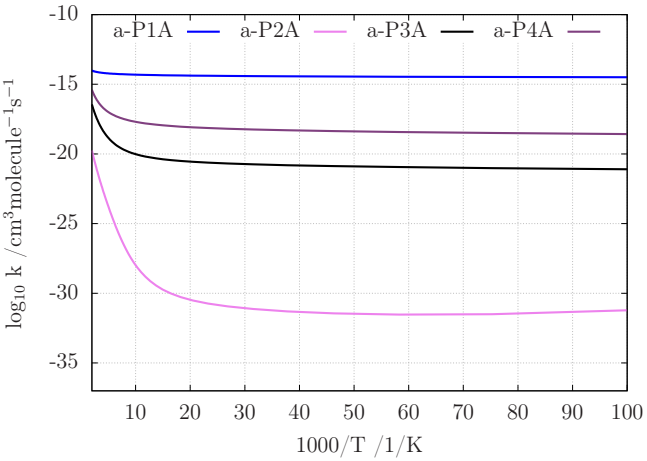

Fig. 8 Arrhenius plot of the formation rate constants of the products a-P1A, a-P2A, a-P3A, a-P4A of the *anti*-VyA + CN abstraction reactions.

Figure 8 shows that also for the abstraction reactions involving the *anti* conformer the fastest process leads to the formation of **a-P1A** in the whole interval of temperatures (10-600 K) and its rate constant ranges between 3.70×10^{-15} and 1.07×10^{-14} $cm^3molecule^{-1}s^{-1}$. The trend of the other rate constants parallels that discussed above for *syn*-VyA, except for the reversal between **a-P3A** and **a-P4A**. Accordingly, the second highest rate constant (ranging between 1.46×10^{-21} and 1.09×10^{-16} $cm^3molecule^{-1}s^{-1}$) governs the formation of **a-P3A**, with the barrier associated to this abstraction process being about 24.0 kJ mol^{-1}. Next, formation of **a-P4A** is governed by an energy barrier of 42.0 kJ mol^{-1} and its rate constant ranges between 4.76×10^{-19} and 9.16×10^{-16} $cm^3molecule^{-1}s^{-1}$. Finally, the slowest process is the formation of **a-P2A**, which is ruled by an energy barrier of 39.7 kJ mol^{-1} and has a rate constant ranging between 4.30×10^{-32} and $6.69\times10^{-20}cm^3molecule^{-1}s^{-1}$.

For addition reactions, the results reported in Figure 9 show that in the whole interval of temperatures (10-600 K) the formation of cyanoacetaldehyde (**P3**) is governed by the highest rate constant, which ranges between 1.40×10^{-10} and $2.40\times10^{-10}cm^3molecule^{-1}s^{-1}$. All the other products are formed by multi-step reaction pathways governed by rate constants decreasing in the order **P6** > **P1** > **P7** > **P5** > **P4** > **P2**, which correspond to vinylcyanide and hydroxyl radical,

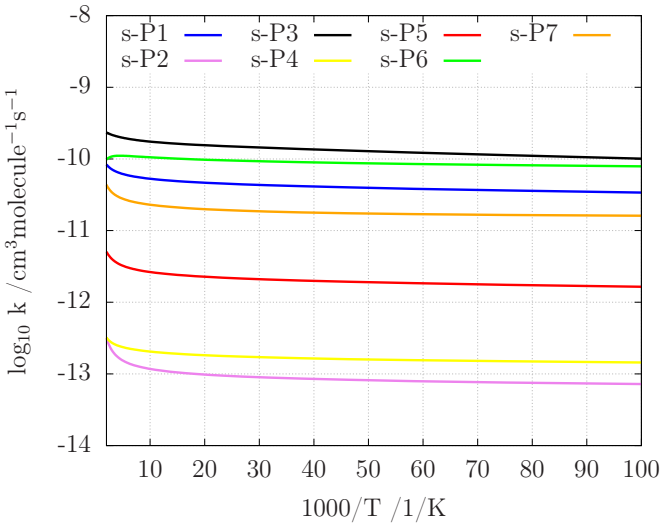

Fig. 9 Arrhenius plot of the formation rate constants of the products s-P1, s-P2, s-P3, s-P4, s-P5, s-P6 and s-P7 of the *syn*-VyA + CN addition reaction.

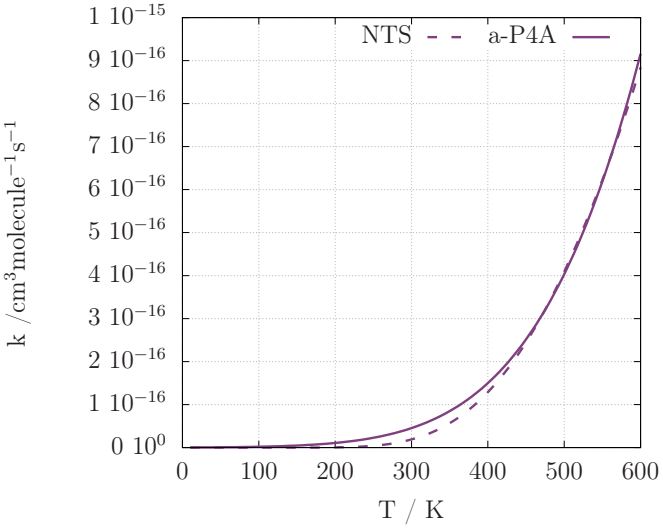

Fig. 11 Comparison between NTS fitting function and computed rate constant for the formation of a-P4 involved in the reaction *anti*-VyA + CN.

(E)-cyanovinylalcohol, (Z)-cyanovinylalcohol, formylcyanide and methyl radical, acetylcyanide, 2-hydroxy-2-propenitrile.

While the general trend of the rate constants governing addition reactions to *anti-Vy* is analogous to that of the *syn* conformer, the reaction pathways discovered by AutoMeKin involve different energy barriers, which lead to non negligible quantitative differences. In any case, the results reported in Figure 10 show that in the whole temperature interval the highest rate constant (between 2.83×10^{-10} and 4.74×10^{-10}cm^{3}molecule^{-1}s^{-1}) governs again the formation of **a-P3**.

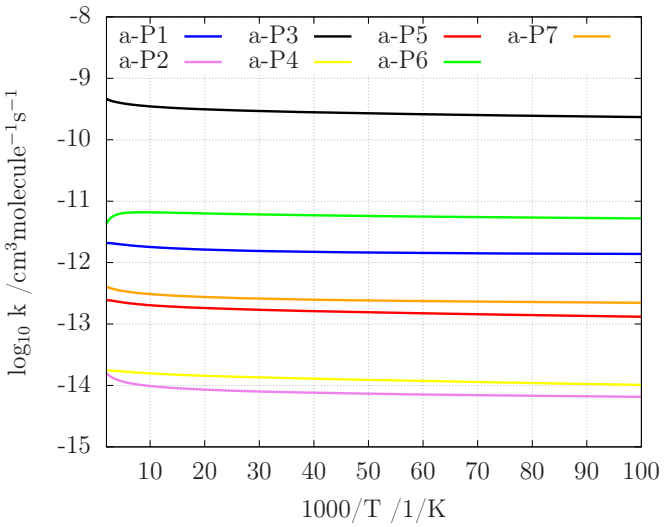

Fig. 10 Arrhenius plot of the formation rate constants of the products a-P1, a-P2, a-P3, a-P4, a-P5, a-P6 and a-P7 of the *anti*-VyA + CN addition reaction.

In summary, the reaction of CN with vinylalcohol leads preferentially to the formation of cyanoacetaldehyde (**P3**) by means of an addition-elimination barrierless reaction. In this case, the ability of the CN radical to further delocalize the π-system of vinylalcohol overcomes the intrinsic preference of the substrate for elimination reactions, which would lead mainly to vinoxy radical and HCN (**a-P1A**). This behavior is reminiscent of that discussed in several papers for the much simpler case of CN addition to ethylene[61–63] and represents the first proposal for a formation route of cyanoacetaldehyde compatible with the harsh conditions of the ISM.

Before concluding this section, let us come back to the role of tunneling in some abstraction reactions. As a matter of fact, in some cases, the Arrhenius-Kooij fittings gave disappointing results at low temperatures. In such circumstances, another more appropriate expression can be used to fit the temperature dependence of the resulting rate constants in the deep tunneling regime, namely the Nakamura-Takayanagi-Sato (NTS)[64,65] expression::

$$k(T) = A\exp\left[-\frac{\varepsilon^{\ddagger}}{R\left(T^2+T_0^2\right)^{\frac{1}{2}}}\right], \qquad (2)$$

in which A, $\varepsilon^{\ddagger}$ and T_0 are the fitting parameters and are defined as pre-exponential factor, the Arrhenius-Eyring energy barrier and the Vogel-Fulcher-Tammann temperature (VFT-temperature), respectively. Figure 11 shows that, contrary to the Arrhenius-Kooij expression, the NTS variant fits fairly well the computed rate constant governing the formation of **a-P4** for the reaction *anti*-VyA + CN.

A deeper insight can be gained by analyzing the so called transitivity ($\gamma(\beta)$), which corresponds to the reciprocal of the activation energy ($1/E_a$) with $\beta = 1/RT$[58]:

$$E_a = -\frac{\partial \ln k(T)}{\partial \beta} \qquad (3)$$

In the case of sub-Arrhenius behaviours typical of low-temperature reactions in which tunneling influences the rate con-

stant, the NTS[64,65] expression can be used to qualitatively analyze the trend of E_a over the temperature range:

$$\gamma(\beta) = \frac{1}{\varepsilon^{\ddagger}} \left[1 + (RT_0)^2 \beta^2\right]^{\frac{3}{2}}$$

Figures 2 and 3 in the Supporting Information show that the NTS function fits very well the transitivity function obtained by the computed rate constants, with this confirming the non negligible role of tunneling at low temperatures for some abstraction reactions and the limitations of the widely employed Arrhenius-Kooij expression in such circumstances.

4 Conclusions

In this work a computational analysis of the mechanism and rate constants for the reaction between the vinyl alcohol and the CN radical has been proposed. In details, the addition and abstraction channels have been analyzed by an automated search for possible reaction mechanisms. After the refinement of the electronic energies of all the stationary points by means of the junChS-F12 composite scheme, a kinetic analysis of all the reaction channels has been performed for the typical temperatures of the ISM.

The results show that the formation of cyanoacetaldehyde (**P3**) is favoured starting from both the *syn* and *anti* conformer of vinyl alcohol in a wide temperature range even if TSs at higher energies are involved with respect to those governing other reaction pathways (see Figure 5 and 6). This apparently surprising trend is due to the presence of low-frequency vibrational motions associated with hindered rotations characterizing several TSs, including **a-TS8** and **s-TS8**, which govern the formation of cyanoacetaldehyde. The presence of very stable reaction intermediates and of several submerged TSs suggests that tunneling cannot decisively condition the value of the rate constants. On the other hand, given that all the species involved in the various mechanisms are strongly excited vibrationally, the effect of the internal rotations of the different TSs plays a decisive role in tuning the final value of the rate constants.

It is noteworthy that the hydrogen abstraction channels are similar to those analyzed by Balucani et al.[63] for the case of ethylene and CN radical. Also in that case the barrierless association is strongly favoured, leading to the formation of thermodynamically very stable reaction intermediates. However, all the hydrogen atoms are equivalent in the case of ethylene with this leading to a single transition state for the hydrogen abstractions, which lies about 5 kJ mol^{-1} above the reactants. In the case of VyA, all the hydrogen atoms are different and this produces four different transition states. The kinetically most favored abstraction process is the one involving the weakest bond (OH), which leads to the formation of **P1A** (i.e., vinoxy radical (CH_2CHO) and HCN) for both VyA conformers.

In our opinion, one of the most interesting outcomes of this study is the proposal of a possible formation route for a prebiotic molecule not yet identified in the ISM, namely cyanoacetaldehyde(**P3**). Actually, the fact that vinylcyanide (issuing from $CN+C_2H_4$) has been detected and cyanoacetaldehyde (possibly issuing from CN+VyA) has not yet been observed could be related to the lack of observations in regions in which both the latter two compounds are present in sufficient concentrations. We therefore suggest to look for cyanoacetaldehyde in those regions where both VyA and CN have been identified, i.e. Sagittarius B2N and G+0.693-0.027.

Author Contributions

B. Ballotta - conceptualization, data curation, methodology, formal analysis, investigation, visualization, writing - original draft, writing review & editing. E. Martínez-Núñez - resources, supervision, software. S. Rampino - supervision, validation. V. Barone - resources, supervision, writing - original draft, writing review & editing.

Conflicts of interest

There are no conflicts of interest to declare.

Acknowledgements

The authors thank Professor Stephen J. Klippenstein of the Argonne National Laboratory and Professor Carlo Cavallotti of the Politecnico of Milan for technical help and enlightening discussions. Funding from the Italian Ministry of University and Research (MUR, Grant 2017A4XRCA) and Italian Space Agency (ASI, 'Life in Space' project N. 2019-3-U.0) is gratefully acknowledged. This work was partially supported by the Consellería de Cultura, Educación e Ordenación Universitaria (Grupo de referencia competitiva ED431C 2021/40), and the Ministerio de Ciencia e Innovación through Grant # PID2019-107307RB-I00. We acknowledge the "Centro de Supercomputación de Galicia" (CESGA) for the use of computer facilities.

Notes and references

1 M. Biczysko, J. Bloino and C. Puzzarini, *WIREs Comput. Mol. Sci.*, 2018, **8**, e1349.
2 S. A. Sandford, M. Nuevo, P. P. Bera and T. J. Lee, *Chem. Rev.*, 2020, **120**, 4616–4659.
3 C. Puzzarini, *Frontiers Astron. Space Sci.*, 2020, **7**, 19.
4 E. Herbst and J. T. J. Yates, *Chem. Rev.*, 2013, **113**, 8707–8709.
5 E. Herbst, *Frontiers Astron. Space Sci.*, 2021, **8**, 776942.
6 V. Barone and C. Puzzarini, *Frontiers Astron. Space Sci.*, 2022, **8**, 255.
7 B. E. Turner and A. J. Apponi, *Astrophys. J.*, 2001, **561**, L207.
8 M. Rodler and A. Bauder, *J. Am. Chem. Soc.*, 1984, **106**, 4025–4028.
9 H. Bunn, K. Hull, I. Miller and P. L. Raston, *J. Phys. Chem. A*, 2020, **124**, 704–710.
10 M. Melosso, B. A. McGuire, F. Tamassia, C. Degli Esposti and L. Dore, *ACS Earth Space Chem.*, 2019, **3**, 1189–1195.
11 V. A. Basiuk and K. Kobayashi, *Int. J. Quantum Chem.*, 2004, **97**, 713–718.
12 N. F. Kleimeier and R. I. Kaiser, *Chem.Phys.Chem.*, 2021, **22**, 1229–1236.
13 C. J. Bennett, Y. Osamura, M. D. Lebar and R. I. Kaiser, *Astrophys. J.*, 2005, **634**, 698.

14 M. J. Abplanalp, S. Gozem, A. I. Krylov, C. N. Shingledecker, E. Herbst and R. I. Kaiser, *Proc. Nat. Acad. Sci.*, 2016, **113**, 7727–7732.

15 B. A. McGuire, *Astrophys. J. Suppl. Ser.*, 2022, **259**, 30.

16 F. Tonolo, J. Lupi, C. Puzzarini and V. Barone, *Astrophys. J.*, 2020, **900**, 85.

17 S. Alessandrini and M. Melosso, *Frontiers Astron. Space Sci.*, 2021, **8**, 754977.

18 C. Puzzarini, Z. Salta, N. Tasinato, J. Lupi, C. Cavallotti and V. Barone, *Monthly Not. Royal Astron. Soc.*, 2020, **496**, 4298–4310.

19 J. Lupi, C. Puzzarini and V. Barone, *Astrophys. J. Lett.*, 2020, **903**, L35.

20 B. Ballotta, T. D. Marforio, S. Rampino, E. Martínez-Núñez, V. Barone, M. Melosso, A. Bottoni and L. Dore, *ACS Earth and Space Chemistry*, 2023, **7**, 1172–1180.

21 V. Barone, J. Lupi, Z. Salta and N. Tasinato, *J. Chem. Theory Comput.*, 2021, **17**, 4913–4928.

22 J. Lupi, S. Alessandrini, V. Barone and C. Puzzarini, *J. Chem. Theory Comput.*, 2021, **17**, 6974–6992.

23 B. Ballotta, S. Nandi, V. Barone and S. Rampino, *ACS Earth Space Chem.*, 2021, **5**, 1071–1082.

24 A. Horn, H. Møllendal and J.-C. Guillemin, *J. Phys. Chem. A*, 2008, **112**, 11009–11016.

25 E. Martínez-Núñez, *J. Comput. Chem.*, 2015, **36**, 222–234.

26 E. Martínez-Núñez, *Phys. Chem. Chem. Phys.*, 2015, **17**, 14912–14921.

27 E. Martínez-Núñez, G. L. Barnes, D. R. Glowacki, S. Kopec, D. Peláez, A. Rodríguez, R. Rodríguez-Fernández, R. J. Shannon, J. J. P. Stewart, P. G. Tahoces and S. A. Vazquez, *J. Comput. Chem.*, 2021, **42**, 2036–2048.

28 K. Fukui, *Acc. Chem. Res.*, 1981, **14**, 363–368.

29 J. J. P. Stewart, *J. Mol. Mod.*, 2013, 1–32.

30 J. J. P. Stewart, *MOPAC2016*, `HTTP://OpenMOPAC.net`.

31 S. Kozuch and J. M. L. Martin, *Phys. Chem. Chem. Phys.*, 2011, **13**, 20104–20107.

32 S. Grimme, S. Ehrlich and L. Goerigk, *J. Comput. Chem.*, 2011, **32**, 1456–1465.

33 E. Papajak, J. Zheng, X. Xu, H. R. Leverentz and D. G. Truhlar, *J. Chem. Theory. Comput.*, 2011, **7**, 3027–3034.

34 D. Garay-Ruiz, M. Álvarez Moreno, C. Bo and E. Martínez-Núñez, *ACS Phys. Chem. Au*, 2022, **2**, 225–236.

35 K. Raghavachari, G. W. Trucks, J. A. Pople and M. Head-Gordon, *Chem. Phys. Lett.*, 1989, **157**, 479 – 483.

36 C. Puzzarini and V. Barone, *Phys. Chem. Chem. Phys.*, 2011, **13**, 7189–7197.

37 C. Puzzarini, M. Biczysko, V. Barone, L. Largo, I. Peña, C. Cabezas and J. L. Alonso, *J. Phys. Chem. Letters*, 2014, **5**, 534–540.

38 S. Alessandrini, V. Barone and C. Puzzarini, *J. Chem. Theory. Comput.*, 2020, **16**, 988–1006.

39 T. H. Dunning, *J. Chem. Phys.*, 1989, **90**, 1007–1023.

40 D. E. Woon and T. H. Dunning, *J. Chem. Phys.*, 1995, **103**, 4572–4585.

41 K. A. Peterson and T. H. Dunning, *J. Chem. Phys.*, 2002, **117**, 10548–10560.

42 V. Barone, S. Di Grande and C. Puzzarini, *Molecules*, 2023, **28**, 913.

43 V. Barone, J. Lupi, Z. Salta and N. Tasinato, *J. Chem. Theory Comput.*, 2023, **19**, doi.org/10.1021/acs.jct.3c00343.

44 J. Bloino, M. Biczysko and V. Barone, *J. Chem Theory Comput.*, 2012, **8**, 1015–1036.

45 M. J. Frisch, G. W. Trucks, H. B. Schlegel, G. E. Scuseria, M. A. Robb, J. R. Cheeseman, G. Scalmani, V. Barone, G. A. Petersson, H. Nakatsuji, X. Li, M. Caricato, A. V. Marenich, J. Bloino, B. G. Janesko, R. Gomperts, B. Mennucci, H. P. Hratchian, J. V. Ortiz, A. F. Izmaylov, J. L. Sonnenberg, D. Williams-Young, F. Ding, F. Lipparini, F. Egidi, J. Goings, B. Peng, A. Petrone, T. Henderson, D. Ranasinghe, V. G. Zakrzewski, J. Gao, N. Rega, G. Zheng, W. Liang, M. Hada, M. Ehara, K. Toyota, R. Fukuda, J. Hasegawa, M. Ishida, T. Nakajima, Y. Honda, O. Kitao, H. Nakai, T. Vreven, K. Throssell, J. A. Montgomery, Jr., J. E. Peralta, F. Ogliaro, M. J. Bearpark, J. J. Heyd, E. N. Brothers, K. N. Kudin, V. N. Staroverov, T. A. Keith, R. Kobayashi, J. Normand, K. Raghavachari, A. P. Rendell, J. C. Burant, S. S. Iyengar, J. Tomasi, M. Cossi, J. M. Millam, M. Klene, C. Adamo, R. Cammi, J. W. Ochterski, R. L. Martin, K. Morokuma, O. Farkas, J. B. Foresman and D. J. Fox, *Gaussian~16 Revision C.01*, 2016, Gaussian Inc. Wallingford CT.

46 H.-J. Werner, P. J. Knowles, G. Knizia, F. R. Manby and M. Schütz, *WIREs Comput. Mol. Sci.*, 2012, **2**, 242–253.

47 H.-J. Werner, P. J. Knowles, F. R. Manby, J. A. Black, K. Doll, A. Heßelmann, D. Kats, A. Köhn, T. Korona, D. A. Kreplin, Q. Ma, T. F. Miller, A. Mitrushchenkov, K. A. Peterson, I. Polyak, G. Rauhut and M. Sibaev, *J. Chem. Phys.*, 2020, **152**, 144107.

48 H.-J. Werner, P. J. Knowles, G. Knizia, F. R. Manby, M. Schütz, P. Celani, W. Györffy, D. Kats, T. Korona, R. Lindh, A. Mitrushenkov, G. Rauhut, K. R. Shamasundar, T. B. Adler, R. D. Amos, S. J. Bennie, A. Bernhardsson, A. Berning, D. L. Cooper, M. J. O. Deegan, A. J. Dobbyn, F. Eckert, E. Goll, C. Hampel, A. Hesselmann, G. Hetzer, T. Hrenar, G. Jansen, C. Köppl, S. J. R. Lee, Y. Liu, A. W. Lloyd, Q. Ma, R. A. Mata, A. J. May, S. J. McNicholas, W. Meyer, T. F. Miller III, M. E. Mura, A. Nicklass, D. P. O'Neill, P. Palmieri, D. Peng, K. Pflüger, R. Pitzer, M. Reiher, T. Shiozaki, H. Stoll, A. J. Stone, R. Tarroni, T. Thorsteinsson, M. Wang and M. Welborn, *MOLPRO, version , a package of ab initio programs*.

49 Y. Georgievskii, J. A. Miller, M. P. Burke and S. J. Klippenstein, *J. Phys. Chem. A*, 2013, **117**, 12146–12154.

50 P. Pechukas and J. C. Light, *J. Chem. Phys.*, 1965, **42**, 3281–3291.

51 W. J. Chesnavich, *J. Chem. Phys.*, 1986, **84**, 2615–2619.

52 A. Fernández-Ramos, J. A. Miller, S. J. Klippenstein and D. G. Truhlar, *Chem. Rev.*, 2006, **106**, 4518–4584.

53 C. Eckart, *Phys. Rev.*, 1930, **35**, 1303–1309.

54 D. M. Kooij, *Zeitschr. Physik. Chem.*, 1893, **12U**, 155–161.

55 K. J. Laidler, *Pure Appl. Chem.*, 1996, **68**, 149–192.
56 A. J. Remijan, J. Hollis, F. Lovas, W. D. Stork, P. Jewell and D. Meier, *Astrophys. J. Lett.*, 2008, **675**, L85.
57 F. Gardner and G. Winnewisser, *Astrophys. J.*, 1975, **195**, L127–L130.
58 V. H. Carvalho-Silva, N. D. Coutinho and V. Aquilanti, *Frontiers in Chemistry*, 2019, **7**, 380.
59 R. P. Bell, *The tunnel effect in chemistry*, Springer, 2013.
60 S. G. Christov, *Quantum Systems in Chemistry and Physics. Trends in Methods and Applications*, 1997, 109–147.
61 K. L. Gannon, D. R. Glowacki, M. A. Blitz, K. J. Hughes, M. J. Pilling and P. W. Seakins, *J. Phys. Chem. A*, 2007, **111**, 6679–6692.
62 G. Saidani, Y. Kalugina, A. Gardez, L. Biennier, R. Georges and F. Lique, *J. Chem. Phys.*, 2013, **138**, 124308.
63 N. Balucani, F. Leonori, R. Petrucci, X. Wang, P. Casavecchia, D. Skouteris, A. F. Albernaz and R. Gargano, *Chem. Phys.*, 2015, **449**, 34–42.
64 K. Nakamura, T. Takayanagi and S. Sato, *Chem. Phys. Lett.*, 1989, **160**, 295–298.
65 S. Sato, *Chem. Phys.*, 2005, **315**, 65–75.